

Rotating Magnetic Nanoparticle Clusters as Microdevices for Drug Delivery

This article was published in the following Dove Press journal:
International Journal of Nanomedicine

Alexander J Willis¹
Sebastian P Pernal²
Zachary A Gaertner³
Sajani S Lakka¹
Michael E Sabo⁴
Francis M Creighton⁴
Herbert H Engelhard⁵

¹Division of Hematology-Oncology, Department of Medicine, The University of Illinois at Chicago, Chicago, IL, USA; ²Wayne State University, Detroit, MI, USA; ³Northwestern University, Chicago, IL, USA; ⁴Pulse Therapeutics, Inc, St. Louis, MO, USA; ⁵Departments of Neurosurgery and Bioengineering, The University of Illinois at Chicago, Chicago, IL, USA

Background: Magnetic nanoparticles (MNPs) hold promise for enhancing delivery of therapeutic agents, either through direct binding or by functioning as miniature propellers. Fluid-filled conduits and reservoirs within the body offer avenues for MNP-enhanced drug delivery. MNP clusters can be rotated and moved across surfaces at clinically relevant distances in response to a rotating magnet. Limited data are available regarding issues affecting MNP delivery by this mechanism, such as adhesion to a cellular wall. Research reported here was initiated to better understand the fundamental principles important for successful implementation of rotational magnetic drug targeting (rMDT).

Methods: Translational movements of four different iron oxide MNPs were tested, in response to rotation (3 Hz) of a neodymium–boron–iron permanent magnet. MNP clusters moved along biomimetic channels of a custom-made acrylic tray, by surface walking. The effects of different distances and cellular coatings on MNP velocity were analyzed using videography. Dyes (as drug surrogates) and the drug etoposide were transported by rotating MNPs along channels over a 10 cm distance.

Results: MNP translational velocities could be predicted from magnetic separation times. Changes in distance or orientation from the magnet produced alterations in MNP velocities. Mean velocities of the fastest MNPs over HeLa, U251, U87, and E297 cells were 0.24 ± 0.02 , 0.26 ± 0.02 , 0.28 ± 0.01 , and 0.18 ± 0.03 cm/sec, respectively. U138 cells showed marked MNP adherence and an 87.1% velocity reduction at 5.5 cm along the channel. Dye delivery helped visualize the effects of MNPs as microdevices for drug delivery. Dye delivery by MNP clusters was 21.7 times faster than by diffusion. MNPs successfully accelerated etoposide delivery, with retention of chemotherapeutic effect.

Conclusion: The in vitro system described here facilitates side-by-side comparisons of drug delivery by rotating MNP clusters, on a human scale. Such microdevices have the potential for augmenting drug delivery in a variety of clinical settings, as proposed.

Keywords: etoposide, glioblastoma, iron oxide nanoparticles, in vitro model, lung cancer, magnetic drug targeting, nanodevice

Introduction

Nanoparticle technology offers ingenious strategies for improving the delivery and targeting of therapeutic molecules for cancer and many other diseases.^{1–6} Magnetic nanoparticles (MNPs) may be used to enhance delivery of chemotherapeutic agents either through direct binding with the agent (which may or may not require a release mechanism), or by functioning as miniature devices (“micro-motors”) for facilitating drug transport via convection or an extended corona effect.^{7–12} Despite the promise of MNPs, successful clinical use of

Correspondence: Herbert H Engelhard
The University of Illinois at Chicago, 912
South Wood St., Chicago, IL 60612, USA
Tel +1 312 996-4842
Email hengelhard@sbcbglobal.net

magnetic drug targeting to date has been rare, underscoring the need for improved in vitro models to bridge the gap “from the bench to the bedside.”^{10–15} In biological applications, individual MNPs tend to aggregate, forming chains and/or clusters.^{16,17} The motion of such structures (under ideal conditions) has been mathematically described.^{18–27} MNP aggregation produces changes in magnetic and physical properties, which may include an enhanced capacity for rotation and translational movement in response to a dynamic magnetic field.^{10,17,26–28}

Most MNPs, and certainly MNP aggregates, would be expected to have limited capacity for moving through solid tissue.^{29–31} However, fluid-filled conduits and reservoirs within the body offer potential avenues for MNP-enhanced drug delivery.^{11,32–34} Within these conduits, factors such as the nature of the transport medium, adhesion to the wall of the conduit, interaction with immune system cells, and distance and angle between the MNPs and the magnetomotive system, will have critical importance in determining the success or failure of the intended therapies. Surprisingly, little data is publically available regarding these specific issues, for systems that employ a rotating magnet for MNP propulsion, especially over human-sized distances.^{10,11,35}

Our group has been investigating a model system that allows MNPs to be “remotely” propelled on a human scale using a rotating permanent magnet.^{10,11,32,34} MNPs synchronously counter-rotate in response to the magnet, act as microscopic stir rods and move by means of surface traction down lanes of specially designed cell culture trays. This surface walking phenomenon has recently been referred to as “magnetically enhanced diffusion (MED)” and “magnetically induced rotation and translation (MIRT).”^{10,11} Use of the parallel “biomimetic” lanes of the tray can be used to facilitate comparisons between different experimental conditions. In two previous publications, we initially described the basic magnet and acrylic tray test configuration,¹⁰ then used it to demonstrate how tissue plasminogen activator (tPA) could be moved to the site of a blood clot in vitro using MNP clusters. In the primitive vascular model, the MNPs could be induced to move even through whole blood.¹¹ As the logical next step, we now address the principles of the system as they pertain to cancer cells, and the delivery of a chemotherapeutic agent.

Here we report our new observations regarding: 1) the relative velocities of different types of rotating MNPs, 2) the effect of magnet position and tray orientation on MNP

velocity, 3) visualization of dye (as a surrogate for drug) movement in response to the MNP clusters, 4) movement of MNPs over monolayers of different cell types, and the resulting adherence to cells, and 5) MNP-facilitated delivery of the chemotherapeutic drug etoposide, as determined by cellular viability testing. Etoposide was chosen because it has been commonly used, has a well-understood mechanism of action, and has been used in the cerebrospinal fluid (CSF).^{32,36} Our hypothesis was that MNP clusters could be used as microdevices to deliver etoposide by means of convection or bulk flow, in the absence of direct etoposide conjugation to the MNPs.

Methods

Magnetic Nanoparticles (MNPs): Synthesis, Size Determination, and Magnetic Separation Time

Four different iron oxide MNPs were tested in initial studies. These are referred to as Fe_3O_4 -MNPs, $\text{Fe}_3\text{O}_4@\text{Au}$ -MNPs, $\text{Fe}_3\text{O}_4@\text{Au-GG}$ -MNPs, and MBs. Synthesis of Fe_3O_4 -MNPs, $\text{Fe}_3\text{O}_4@\text{Au}$ -MNPs, and $\text{Fe}_3\text{O}_4@\text{Au-GG}$ -MNPs was according to Venugopal et al.³⁷ For this synthesis, all chemicals were purchased from MilliporeSigma (Burlington, MA) with the exception of hydrogen tetrachloroaurate (III) hydrate, which was purchased from Alfa Aesar (Haverhill, MA). Magnetic microbeads (MBs) were provided by Pulse Therapeutics, Inc. (St. Louis, MO), and have recently been described.^{10,11,32} MBs are ferrimagnetic, with single-crystalline magnetite cores. The volume of MNP suspensions used in experiments described here was 20 μL (or 100 μL), from stock solutions of 25 mg/mL, unless otherwise noted.

For MNP synthesis, 3.46 g of iron (III) chloride hexahydrate ($\text{FeCl}_3 \cdot 6\text{H}_2\text{O}$) and 1.27 g of iron (II) chloride ($\text{FeCl}_2 \cdot 4\text{H}_2\text{O}$) were dissolved in 100 mL of 0.40 M hydrochloric acid aqueous solution (HCl_{aq}) to make the iron stock solution. The molar concentrations of the two iron salts in the solution were 0.128 M iron (III) and 0.064 M iron (II), respectively. Three mL of 1 M TX-100 solution was added to 250 mL of 1 M aqueous sodium hydroxide (NaOH), then heated to 75°C in a water bath. Twenty-five mL of the iron stock solution was added dropwise into this solution under vigorous non-magnetic stirring. After complete addition of the stock solution, the stirring was continued for 20 mins at 75°C. The Fe_3O_4 magnetic cores obtained were allowed to settle before magnetic separation, to remove the supernatant. These particles were then washed

multiple times with distilled water to remove excess surfactant, then resuspended in distilled water, and designated “Fe₃O₄”.

For coating these MNPs with gold, 1 g of gold (III) chloride trihydrate was dissolved in 1 mL of dH₂O, while being protected from light, to create a gold-coating solution. Ten mL of the 25 mg/mL Fe₃O₄-MNP solution was transferred to a 150 mL beaker, and 90 mL of dH₂O was added for a total volume of 100 mL. 0.5 g of D (+) glucose was added to the iron core solution and sonicated for 15 mins before being placed in a 60°C water bath. Once the iron core solution reached 60°C, the gold-coating solution was added at a molar ratio of 1:2, then slowly stirred for 1 hr with non-magnetic stirring, protected from light. Gold-coated MNPs were transferred to a 50 mL Falcon tube (Corning, Corning, NY) and washed three times with dH₂O, with vortexing, sonication for 30 sec, and magnetic separation each time. The resulting “Fe₃O₄@Au” particles were stored in dH₂O at 25 mg/mL at room temperature (RT).

For the production of “Fe₃O₄@Au-GG” particles, an aqueous solution of gellan gum (Phytigel™) was prepared by slow addition of 5 mg of Phytigel™ to 90 mL of water while heating using a magnetic stirring hotplate. Water was added until the solution volume reached 100 mL, and the pH was adjusted to 10 by dropwise addition of 1 M NaOH. This was then heated to 70°C while being stirred. After removing from heat, 3 mL of Fe₃O₄@Au -MNPs was added dropwise to the gellan gum solution while it was undergoing non-magnetic stirring. The solution was cooled to RT and stirred for an additional 1 hr, then washed and stored as described above.

MNP size determinations were performed using the Nanosight LM10, using the Nanosight NTA 3.0 software (Malvern, Malvern, UK). MNPs were prepared for analysis at a concentration of 1 mg/mL in PBS, then further diluted 1:100 to 10 ug/mL of MNPs. Directly prior to loading, the solution was sonicated using the Sonics Vibra-Cell (Sonics, Newton, CT). Nanoparticle motion was tracked for 30 sec in triplicate. For magnetic separation times, the Lifesep Series Biomagnetic Separator (Dexter Magnetic Technologies, Elk Grove Village, IL) was used, which was also used for MNP washing. Twenty-five mg of each MNP was loaded into separate 50 mL Falcon tubes suspended in 10 mL of phosphate-buffered saline (PBS), which were then placed into the magnetic separator. The clearance of the MNPs was video recorded using an Olympus SZ-12 camera (Olympus Corp., Center Valley, PA). The videos were analyzed using

Quicktime (Apple Inc., Cupertino, CA). Separation time was measured in seconds. For CT and MRI imaging, evenly dispersed dilutions of MNPs were made in 5 mL of warm 2.5% agarose, and scanned in 12-well plates (Falcon) after refrigeration for 10 mins to harden the gel.

Rotating Permanent Magnet System (Mini-MED) and Acrylic Trays

The dynamic magnetic field used in these studies was generated by a rotating permanent magnet system (“mini-MED”) provided by Pulse Therapeutics, Inc. (St. Louis, MO). This contains a neodymium-boron-iron permanent magnet (US patents 8,313,422, 8,308,628, and 8,529,428), which spins in one direction at 3 Hz, causing agglomerated MNPs to synchronously rotate and surface walk even when separated at a distance from the magnet. The mini-Med has recently been described in detail.^{10,11,32,34}

Poly (methyl methacrylate) acrylic trays for testing the movement of MNPs by the mini-MED, were designed and produced as previously described.^{10,11,32,34} These trays (US patent applied for), were specifically designed to study the magnetically induced rotation and translation (MIRT) of MNPs. MIRT trays are compatible with standard 96-well plate readers, as well as inverted microscopes, and therefore can also be utilized for fluorescence or dye studies. Each smooth, rounded lane in the straight lane tray is 1/8th inch (3.175 mm) wide. Here, a tray with a branching pattern was also used for dye studies. When used for tissue culture, trays were sterilized overnight using ethylene oxide, or with 100% ethanol and UV light.

Figure 1A shows a CAD image used in the design of the straight lane MIRT trays. Figure 1B is a photograph of a MIRT tray mounted on a plexiglass plate, over the mini-Med, in the offset above position (at a height of 20 cm). Figure 1C is a photograph of a portion of the tray, showing three of the eight lanes loaded with MBs (the most easily seen MNP) at their starting points, before the initiation of the rotation and translational movement resulting from starting the rotation of the magnet.

Standard Tray Positions and Video Determination of MNP Velocity; Colored Dye Analysis

A diagram illustrating the different tray positions used for this paper is seen in Figure 2. The origins or starting points for the MNPs (from the vantage point of this figure), were always to the left. From this view, MNPs

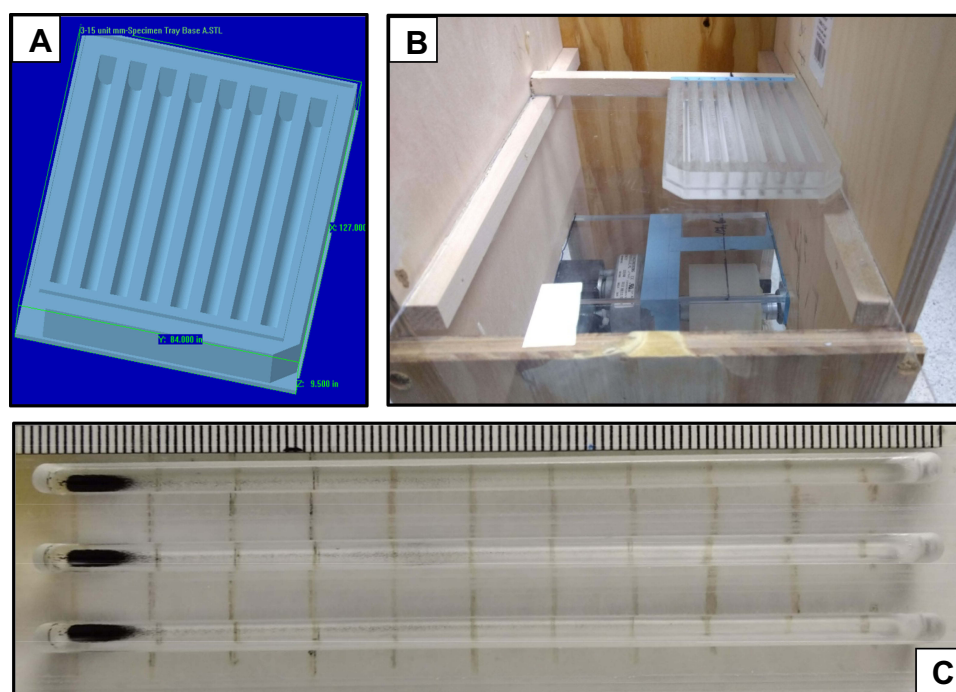


Figure 1 (A) CAD image used in the design of the “magnetically induced rotation and translation (MIRT)” trays. The lanes have rounded bottoms to simulate tubular conduits within the body. (B) Photograph of the MIRT tray mounted on a plexiglass plate, over the mini-Med magnet, in the offset above position (at a height of 20 cm). (C) Photograph of a portion of the tray, showing three lanes (or channels) loaded with MNPs at their starting points, before the initiation of the rotation and translational movement induced by activating the mini-MED. Use of the tray lanes can be used to facilitate side-by-side comparisons of different types of MNPs, MNP modifications, the addition of drugs, or alterations of the media and cells within the channels. The tray is compatible with a standard 96-well plate reader.

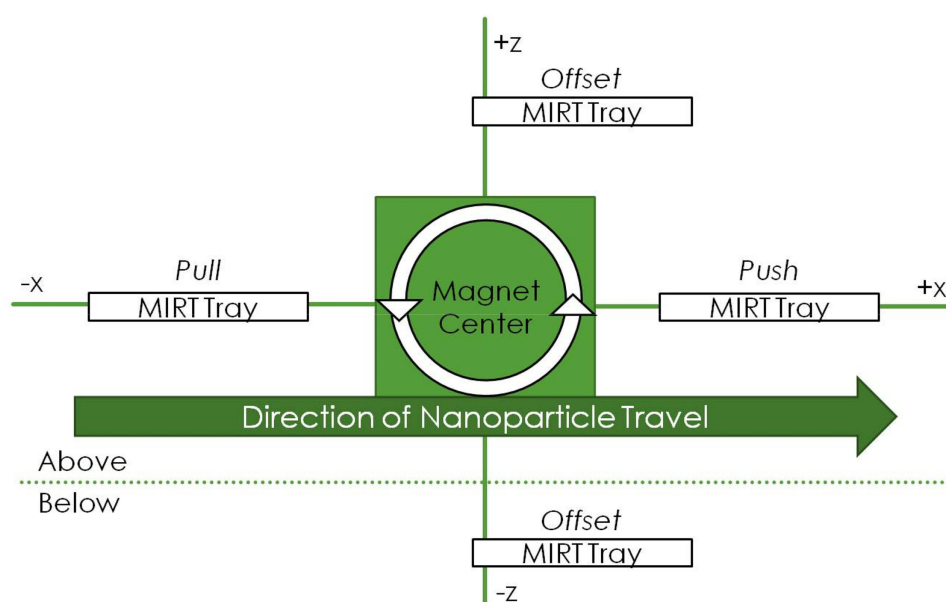


Figure 2 Schematic illustrating the standardized MIRT tray positions used in this paper. This perspective is rotated 90 degrees to the left, from that shown in Figure 1B. The figure is not drawn to scale: in actuality, the tray in the pull position would be relatively closer to the rotating magnet, if the starting positions for the MNPs were all 20 cm from the center of the magnet.

moved to the right, whether above or below the magnet, due to the influence of the mini-MED rotation. Use of these standardized tray positions (designated “pull”,

“push”, “offset” and “offset below”) allowed comparisons to be made between MNP “runs,” and avoided non-movement areas that might be created by the formation

of magnetic cancellation nodes.³⁸ For some experiments, additional vertical stacking heights were added to the basic tray position.

Digital videos of MNPs being moved (in horizontal translation) by the mini-MED in the MIRT trays were made using an Olympus SZ-12 camera (Center Valley, PA). An “average” velocity determination for MNPs running down a lane was simply calculated from the MNP run time for the entire lane (distance: 10 cm). Velocity values in cm by cm analyses were calculated using MATLAB’s Video Viewer application (MathWorks, Natick, MA). As the leading edge of the MNP cluster passed each marked centimeter, the frame number was recorded. The difference in frames from cm to cm was divided by the frame rate (29.97 frames/sec) to determine the time for that particular span. The distance (i.e. 1 cm) was divided by the time to determine the velocity in cm increments. MNP acceleration was calculated by dividing the change in velocity readings over a given span, by the elapsed time.

In the cell-free system, MNP velocity was usually measured using 1 mL per lane of PBS at RT. 20 μ L of 25 mg/mL MNP solution was added to the starting points (i.e. origins) of the lanes of the tray. MNPs were pre-magnetized by placing the tray at the side of the magnet, which consolidated the MNPs at each lane origin. The tray was then mounted at the position of interest, so that the median of imaged lanes would be along the central plane of the magnet. MBs were chosen over other MNPs for more extensive studies, since they had the greatest velocity in response to the mini-MED (as detailed in the Results section below). This improved velocity profile (other factors being equal) would be expected to convey an advantage in any future clinical setting. MB translation in the branched lane MIRT tray was studied using 8 mL of PBS, with 50 μ L of 25 mg/mL MB solution being added to the starting point, again with pre-magnetization prior to the run.

Since most drugs are transparent, commercially available dyes (food coloring, trypan blue) were used to directly visualize the effects of MNP clusters on the movement of small molecules. Lanes of the straight lane tray were loaded with pre-mixed MNPs+yellow dye, versus 5 μ L of yellow dye alone (which would indicate diffusion). Lanes were also loaded with 5 μ L of blue dye placed 6 cm from the tray origin. Dye studies were performed with the magnet in the “pull” position. For branched lane studies, MNPs pre-mixed with yellow or blue dye were added to their respective lanes. Trypan

blue was obtained from Lonza (Basel, Switzerland). To study the effect of trypan blue (molecular weight 872.88) on MB aggregation, 5 μ L of trypan blue was added to 20 μ L of 25 mg/mL of MBs, and the suspension vortexed for 30 sec, before being placed on a slide for photography. The effect of trypan blue on MB velocity was studied in the straight lane MIRT tray, using various tray positions.

Cell Culture, Staining, and Microscopy

Cell lines used in these experiments were obtained from the American Type Tissue Collection (Manassas, VA), along with E297 (DOI 10.1097/00006123-200103000-00035) and LKB1-KO (Jackson Laboratory, Bar Harbor, ME) cells. Cells were maintained using standard tissue culture technique at 37°C in 5% CO₂. HeLa cells were grown in MEM (Thermo Fisher, Waltham, MA.), and H2122 cells were grown in RPMI 1640 (Thermo Fisher, Waltham, MA). All other cells were grown in DMEM (Thermo Fisher, Waltham, MA). Cells were supplemented with 10% FBS (Thermo Fisher, Waltham, MA.), 1% Pen/Strep solution (Corning Inc., Corning, NY.), and 1% Ciprofloxacin (1 mg/mL) (Corning Inc., Corning, NY).

Cells were imaged either in 12-well culture plates, or MIRT trays, depending on the experiment. Phase-contrast images were obtained with an inverted microscope at 10 \times (Nikon Corp., Tokyo, Japan). For fluorescence or H&E staining, cells were washed with PBS before being fixed in 4% paraformaldehyde for 10 mins at RT, and washed again. Nuclei were stained in the MIRT tray by addition of 1 mL of Hoescht 33342 in PBS (1:1000 v/v; Sigma-Aldrich, St. Louis, MO) for 10 mins at 37°C. Cells in the MIRT tray were imaged using an EVOS FL Auto 2 microscope (Fisher Scientific, Waltham, MA). For scanning electron microscopy (SEM), samples were dehydrated using ethanol then hexamethyldisilazane. Glass cover slips were adhered to aluminum mounts with double-sided sticky tape and sputter coated with 6.0 nm of Pt/Pd in a low-pressure argon atmosphere for conductivity. Surfaces were analyzed at the UIC Electron Microscopy Service facility (Research Resource Center). Morphology was examined using a Hitachi S-3000N Variable Pressure Scanning Electron Microscope using secondary (SE) and backscatter (BSE) detectors.

For cell adhesion studies, cell lines were grown in 6 well plates to confluence, then treated with 1 mL of 10 μ g/mL MBs for 30 mins at 37°C, then washed three times with PBS to

eliminate non-adherent MBs. Images obtained by the inverted microscope were converted into binary files, and analyzed using ImageJ (National Institutes of Health) to quantify the relative number of MBs adhering to cells. For MIRT tray studies of MB velocities over cells, 1×10^5 cells were seeded into each lane of the sterilized MIRT tray, which were pre-coated with 1 mL of 0.1% gelatin and incubated at 37°C for 15 min. Cells were grown for 24–48 hrs (until confluent) before further experimentation. Immediately prior to velocity determinations, the medium was replaced with 1 mL of PBS.

Evaluation of MB Delivery of Etoposide, by MTT Assay and Trypan Blue Exclusion

Since MBs were the fastest MNP, experiments were designed to determine whether or not they could be used to deliver a chemotherapeutic drug (etoposide), in the absence of direct conjugation to the drug. Etoposide was purchased from Cayman Chemical Company (Ann Arbor, MI), and stored at –20°C. Etoposide dilutions were made from a stock solution of 1 mg/mL in DMSO. The direct cytotoxic effects of different concentrations of etoposide (ranging from 1 to 100 μ M) were studied prior to MB testing. Baseline (static) studies were performed in 12-well culture plates, with direct treatment of cells (U138 and H2122) in monolayer culture, using 1) etoposide alone, 2) MBs alone, or 3) a combination of MBs with etoposide, in comparison to untreated control cells. In these static studies, no magnet was used.

Standard MTT assays were performed in 12-well plates, as previously described.³⁹ Cells were seeded at a density of 10^5 cells per well and grown for 24 hrs then treated for 24 hrs. Thiazolyl blue tetrazolium bromide powder (MilliporeSigma, Burlington, MA) was dissolved in 1X PBS at a concentration of 5 mg/mL to make the MTT working solution, which was diluted in media at 10% v/v. After cells had grown for 24 hrs, media was aspirated, cells were gently washed 3 times with 200 μ L PBS, fresh media was added, and a 100 μ L treatment volume was applied. After incubation at 37°C in 5% CO₂ for 24 hrs, media was aspirated, MTT-media was added, and cells were incubated at 37°C (5% CO₂) for 4 hrs. The MTT-media was aspirated, DMSO was added, and cells were incubated at 37°C for 30 mins. The resulting solution was transferred to 96-well plates in triplicate and read with a SPECTRAMax 340PC (Molecular Devices, San Jose, CA) at 590 nm in triplicate.

Translational (i.e. dynamic) experiments were then performed to determine whether or not etoposide could be transported 10 cm down the length of the MIRT tray by MB clusters in response to the mini-MED. The straight lane MIRT tray in the 20 cm pull position was used. Sixty μ L of MBs alone and 60 μ L of MBs plus 100 μ M etoposide were loaded at the starting points of the tray. The mini-MED was turned on (“activated”) for 5 mins to ensure that all MBs had traveled the complete distance of the tray. Four hundred μ L of MB solution was removed from the end of each lane and transferred to an Eppendorf tube. One hundred μ L of this solution was applied to wells of a pre-seeded 12-well culture tray (U138 and H2122; 10^5 cells/well, 24 hrs), in triplicate. After a treatment time of 2 hrs at 37°C in 5% CO₂, the supernatant (including any dead cells) was transferred into a 15 mL Falcon tube (Corning, Inc., Corning, NY) and 1 mL of media was added per well in order to harvest the remaining cells. Cells were detached with gentle use of a cell scraper and added to the 15 mL tube, which was centrifuged at 1800 rpm for 5 mins. Cell pellets were resuspended in 1 mL of media. One hundred μ L of cell suspension was added to 400 μ L of trypan blue. Ten μ L of trypan blue cell suspension was then transferred to a hemocytometer, and live and dead cells were counted, with counts being performed 5 times per group.

Data Display and Tests of Statistical Significance

Data (e.g. the velocity curves) are expressed as mean and standard deviation (mean \pm SEM) with n values as given in the text and/or figure legends. Statistical significance for the velocity and absorbance experiments was determined using two-factor ANOVA with replication. A value of $p < 0.05$ was considered to be statistically significant.

Results

Comparison of MNP Types: Magnetic Separation Times, Translational Velocities, and Particle Sizes

In initial studies, the magnetic separation times for the four different MNPs in PBS were determined using the biomagnetic separator. Results are shown in Figure 3A. MBs had the fastest clearing time (approximately 5 sec) due to their greater magnetic dipole moment. The movement of the four types of MNPs in the MIRT tray in response to the rotating permanent magnet (mini-MED) was then studied. MNPs

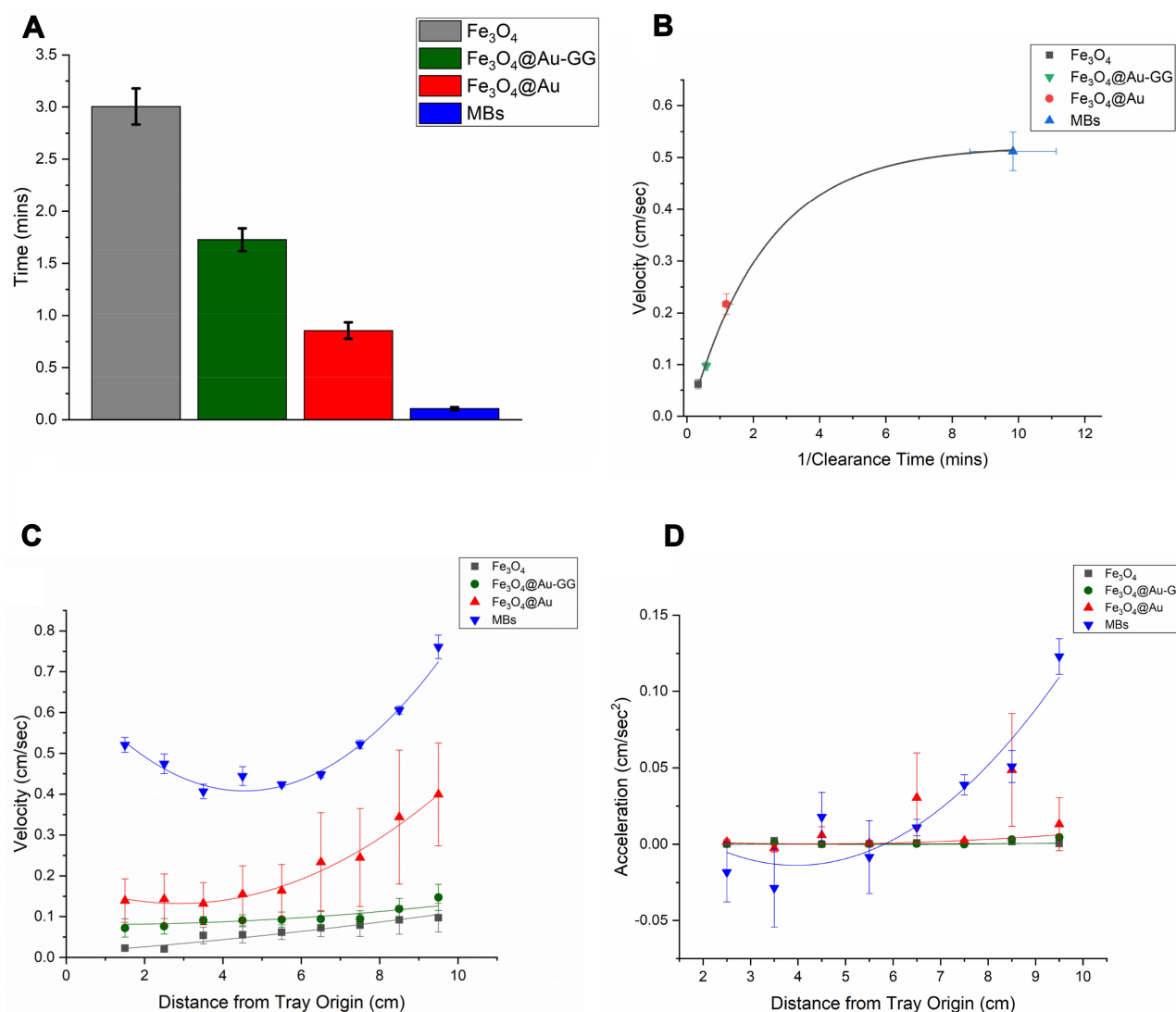


Figure 3 (A) Comparison of the magnetic separation times of the four different MNPs ($n=3$). (B) Average MIRT tray velocity (pull position) plotted as a function of the inverse of magnetic separation (clearance) time. The MBs separate most quickly and move the fastest in the MIRT tray. (C) MNP velocities plotted centimeter by centimeter as they move down the tray, in the pull position, showing the differences according to particle type ($n\geq 3$). (D) MNP acceleration, in the pull position, showing the greater acceleration as particles approach the magnet as demonstrated by the MBs.

form clusters in response to a magnetic field. MNP clusters counter-rotate and act as microscopic stir rods, in response to a rotating magnetic field, resulting in the surface-walking phenomenon at a distance from the magnet. Here, PBS was used as the transport media, and the pull position for the tray was used (as illustrated in Figure 2), with a starting distance of 20 cm from the magnet center. Not unexpectedly, the MBs moved the fastest in this situation as well, traversing a centimeter in approximately 2 seconds. Average velocities were plotted against the inverse of the magnetic separation times for the four MNPs, as shown in Figure 3B. Videography and digital analysis allowed for accurate quantification of MNP velocities, cm by cm, as they moved down the lanes of the MIRT tray.

Use of the parallel lanes was used to facilitate side-by-side comparisons of MNP translational velocities and cluster dispersion, according to particle type/coating. A plot of MIRT tray velocity versus distance from the tray origin for the different formulations, can be seen (for the pull position) in Figure 3C. With this tray position, MNPs accelerate due to the addition of the force of attraction to the permanent magnet, to the velocity produced by cluster rotation and surface traction, as the MNPs approach the mini-MED. This is shown in Figure 3D, which is a plot of particle acceleration as a function of distance down the tray.

MNP sizes were determined using the Nanosight LM10 instrument and NTA 3.0 software. Mean

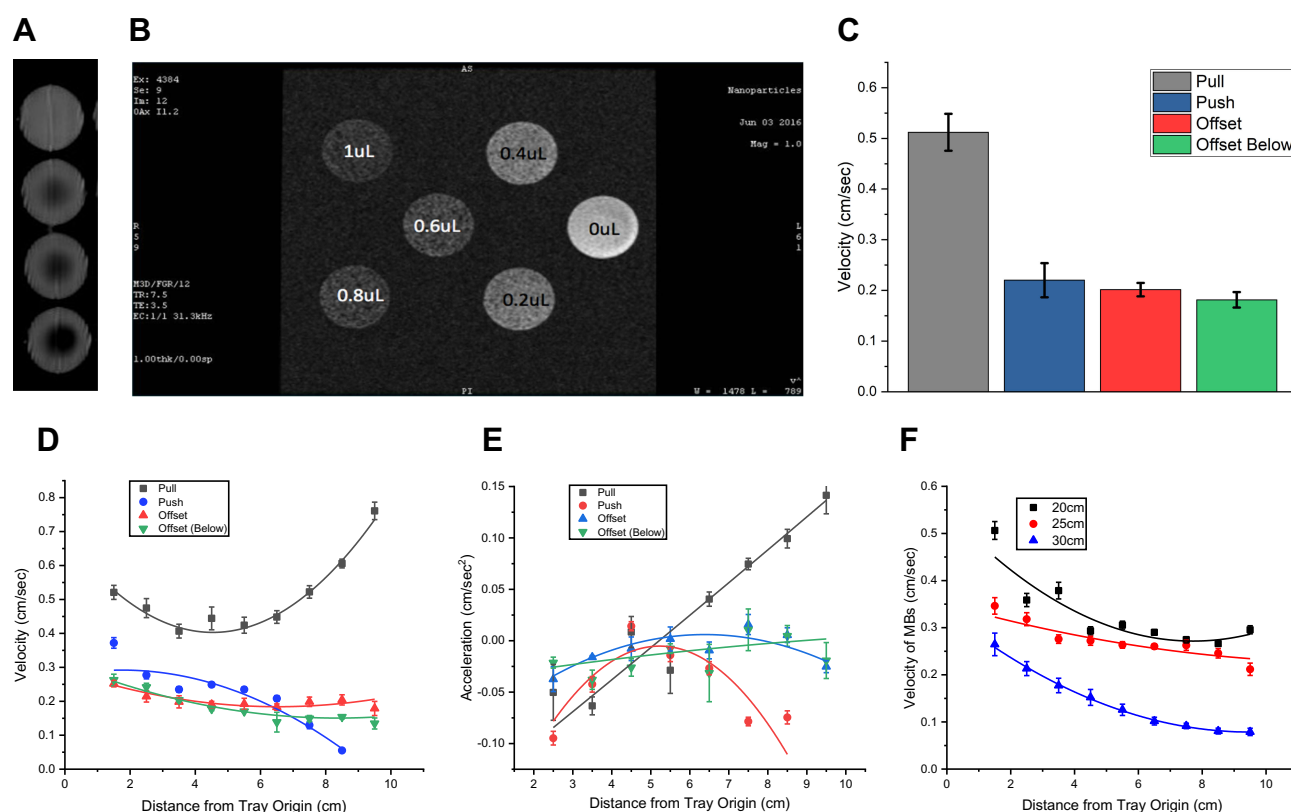


Figure 4 (A) CT images of 0–500 μ L of agarose-embedded MBs in tissue culture wells. (B) Ultrafast gradient-echo MR images of agarose-embedded MBs, with concentrations as indicated. Here, use of adjacent wells was avoided, in order to avoid imaging artifacts. (C) Average MB velocity according to tray position ($n > 3$). MBs moved fastest in the pull position. (D) MB velocity according to tray position, centimeter by centimeter, as determined by video analysis. In the pull position, they accelerate as they approach the magnet; in the push position, velocity falls off. (E) MB acceleration according to tray position, which similarly shows the greatest acceleration close to the magnet, and acceleration decreasing in the push position farther away from the magnet. (F) Velocities of MBs in the offset above position, with the tray at three different heights above the mini-MED ($n = 9$). As expected, increasing the distance from the rotating magnet resulted in decreased velocities of the particles.

diameters for Fe_3O_4 , $\text{Fe}_3\text{O}_4@\text{Au}$, and $\text{Fe}_3\text{O}_4@\text{Au-GG}$ – MNPs were 95.4 ± 20.0 , 105.9 ± 15.1 and 109.2 ± 9.7 nm, respectively, which indicated that the sequential coating process with gold and then gellan gum was successful and increased the particle diameter. Solitary MBs have a mean diameter of 60 nm and are prepared differently.^{10,11,32} Translational velocity was therefore not just a function of particle core size. Based on these results, the MBs were used for further studies, due to their greater velocities and capacity for movement at greater distances from the mini-MED. Pre-magnetizing the MBs (by exposing them to the magnet prior to initiating magnet rotation) increased MB velocities, and was used as part of the standard procedure for subsequent experiments. MBs can be visualized radiographically, by x-ray, CT scan, and MRI. CT and MR images of MB dilutions (as indicated) are seen in Figure 4A and B. MRI, as expected, was found to be far more sensitive for MB detection than CT, especially when using T2-weighted or ultrafast gradient-echo imaging.

Effect of MIRT Tray Position on MB Velocity

Changing the position (and/or distance) of the MIRT tray relative to the mini-MED changed the velocities of the MNPs – an important consideration (of course) when considering moving from in vitro to animal or especially human use. In data presented here, all tray positions were centered in the plane of the rotating magnetic field (as shown in Figure 2). Figure 4C shows average MB velocities in the four key positions: pull, push, offset and offset below. The standard starting point (origin) from the magnet center was 20 cm in all positions shown. The pull position produced the greatest average velocity. MNPs placed in a tray directly above the magnet (not offset) demonstrated complex patterns of motion, due to the combination of “pull” and “push” effects.

Figure 4D shows MB velocities centimeter by centimeter, as they move down the lanes of the MIRT tray. MB clusters seem to oscillate, with some expansion and

contraction as they moved down the lane. MB velocity increases in the pull position at the end of the lane, since particles are approaching the magnet. This was confirmed in the acceleration plot, as seen in Figure 4E. Determinations were made to see how the amount of MBs used (i.e. aliquot size) affected their velocity, and whether lane position (e.g. lane 1 versus lane 3) was a factor in MB velocity, such as due to lack of homogeneity in the magnetic field. These results are shown in Table 1. While the effect of lane position on MB velocity was not found to be statistically significant, larger MB aliquots (100 μ L in comparison to 20 μ L) did indeed have greater velocities, especially in the pull position. Increasing the distance of the tray from the mini-MED resulted in decreased velocities as expected, as seen in Figure 4F, for the offset (above) position.

Dye Diffusion versus Magnetically Enhanced Dye Delivery

In order to model the effect of MBs on delivering a drug to a target area (through a conduit), studies with yellow and blue dyes were performed. Most drugs are transparent, but fluorescent drugs, or tagged therapeutic molecules, can also be studied in this fashion since the MIRT tray is compatible with standard 96-well plate readers. MBs (acting in response to the rotating magnet) were found to greatly accelerate dye delivery, when compared to diffusion alone. An example of this effect is illustrated in Figure 5A and B, for a cell-free system. Six lanes of the straight lane MIRT tray are shown, each of which contains yellow dye (representing drug) and blue dye (representing the target). Figure 5A is a photograph of the tray immediately after loading and initiating MB rotation with the mini-MED. Figure 5B shows the dispersion of the dye 30 sec later, when the MBs contact the target region. Successful dye delivery was confirmed once green coloring appeared.

The average velocity of the yellow dye as propelled by the MBs (0.18 ± 0.01 cm/sec), versus by diffusion alone (0.005 ± 0.0006 cm/sec), is graphed in Figure 5C. ANOVA two-factor analysis with replication showed that these values are statistically different, with $p < 0.05$. In both situations, dye does become diluted with movement down the lanes of the tray. MBs were able to transport dye (as a drug surrogate) in a branched lane tray as well, as illustrated in Figure 5D. Dye delivery could therefore be used to visualize the effect of MNPs as microdevices for drug delivery (i.e. by convection or bulk flow), in the absence of direct conjugation to the particles. MB-facilitated movement of trypan blue dye also studied. Trypan blue, which is negatively charged, inhibited the formation of MB aggregates when vortexed with MBs, as seen in Figure 5E and F. Combining MBs with trypan blue, did slow translational velocity somewhat, depending on tray position. Individual dyes were therefore found to respond differently in the model system, according to factors such as size, concentration, and surface charge, and the same would be anticipated for different drugs.

Movement of MBs Over Cellular Monolayers and Adherence of MBs to Cells

Interaction of MBs with cells cultured in monolayers was then studied, for several different cell lines, including HeLa (cervical cancer), human glioblastoma lines, and LKB1-KO. Different MB volumes, and cellular confluence percentages, were tested. MBs placed at the edge of a monolayer of cells in a standard 6-well plate, then exposed to the action of the mini-MED, tended to fan out to both sides, as seen in Figure 6A. Effects resulting from proximity to the side of the well, and at the fluid meniscus, were also observed. MBs were seen to adhere differently to different types of cells forming a confluent monolayer. Phase-contrast microphotographs, and images of cells stained with hematoxylin and eosin, are

Table 1 Effect of Lane Position (Pull vs Offset Above) and Aliquot Size (20 vs 100 μ L) on Average Velocity of MB Clusters

20 μ L Pull	Average Velocity	SEM	20 μ L Offset	Average Velocity	SEM
Inner	0.421	0.0513	Inner	0.228	0.0095
Middle	0.412	0.0516	Middle	0.187	0.0071
Outer	0.419	0.0463	Outer	0.189	0.0067
100 μ L Pull	Average Velocity	SEM	100 μ L Offset	Average Velocity	SEM
Inner	0.653	0.0762	Inner	0.241	0.0174
Middle	0.621	0.0896	Middle	0.232	0.0125
Outer	0.624	0.0826	Outer	0.215	0.0131

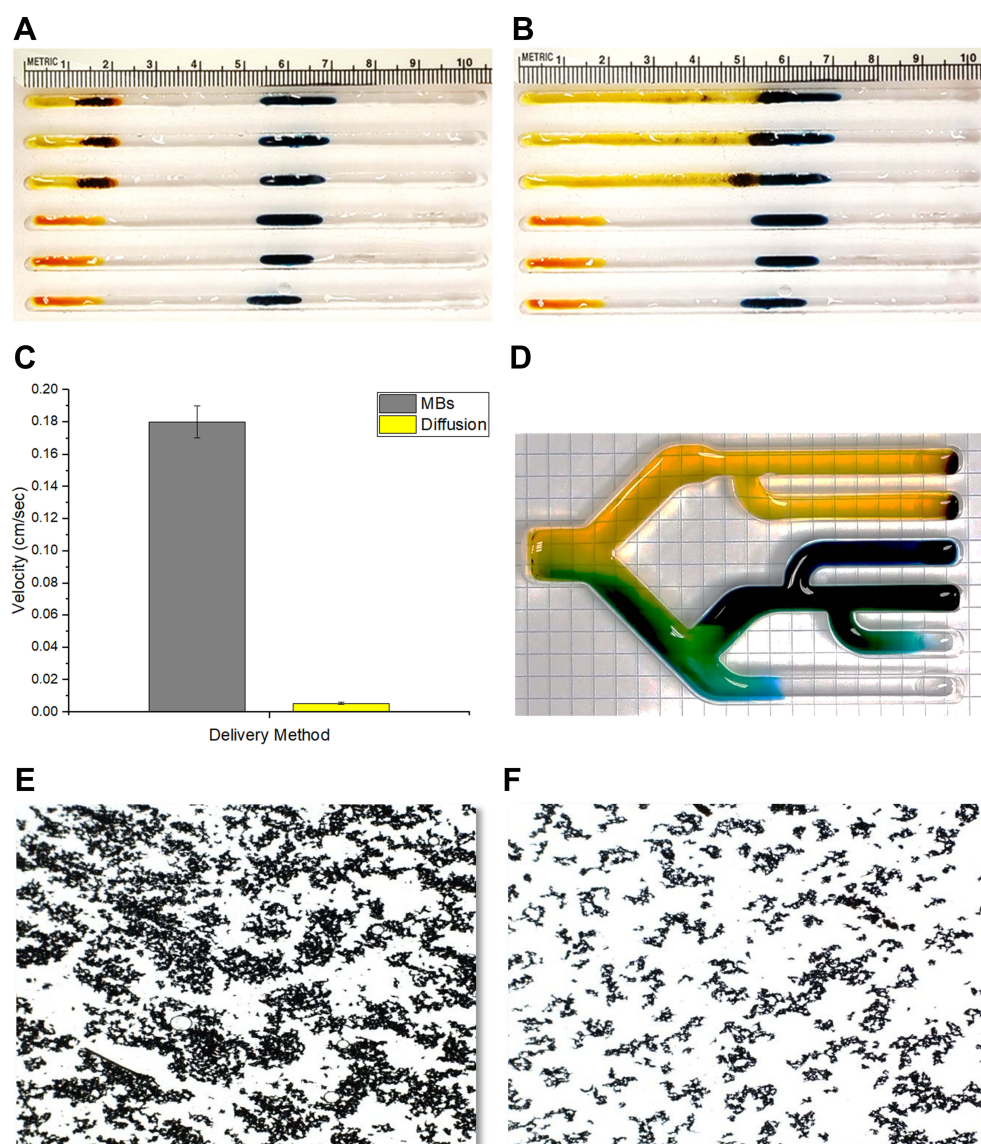


Figure 5 (A and B) A comparison of dye diffusion versus magnetically enhanced dye delivery, as demonstrated in the MIRT tray. (A) Positions of MBs with dye (top three lanes) and dye samples alone (bottom three lanes) at the time of mini-MED activation, with blue dye targets in the central portion of the tray. (B) Positions 30 sec later, when the MBs bring the yellow dye into contact with the blue target region (top three lanes), versus dye diffusion proceeding without MBs (bottom three lanes). (C) Bar graph showing a comparison of the velocities of MB-induced dye delivery versus movement by diffusion alone (n=3). (D) Photograph showing dye movement in response to MBs in a branched tray system, after 15 mins of mini-MED activation. MBs drag blue and yellow dyes (as drug surrogates) along with them, which then co-mingle to form green. (E and F) Effect of trypan blue dye on MB dispersion. (E) Photomicrograph of MBs in PBS. (F) Photomicrograph of MBs in PBS with addition of trypan blue, showing the resulting increase in particle dispersion (10× magnification).

shown in Figure 6B and C, respectively. A scanning electron microscope (SEM) image of an MNP cluster on a glioblastoma cell is seen in Figure 6D. $\text{Fe}_3\text{O}_4\text{@Au}$ -MNPs were less toxic than Fe_3O_4 -MNPs, at a treatment time of 24 hrs. No evidence was observed of any significant cellular toxicity resulting from exposure to MBs. Image J was used to quantify MB adhesion to the cancer cells after cell washes, with results shown in Figure 6E. MBs were seen to be more adherent to live cell monolayers than to paraformaldehyde-fixed cells, and more adherent (in general) to cancer cells than non-neoplastic

cells. Figure 6E shows MB adherence to live and fixed glioma cells, versus cultured non-neoplastic astrocytes.

Cells were then grown in the lanes of the MIRT tray, in order to channel the translational movement produced by the mini-MED, as could be utilized in order to transport MNPs within physiologic conduits inside the body (such as blood vessels, the spinal subarachnoid space, ureters, lymphatics, etc.) Our data on vascular cells have been recently reported.¹¹ Cells were found to grow better in trays milled from acrylic, than in trays 3D printed in VeroClear. Bits of the poly (methyl

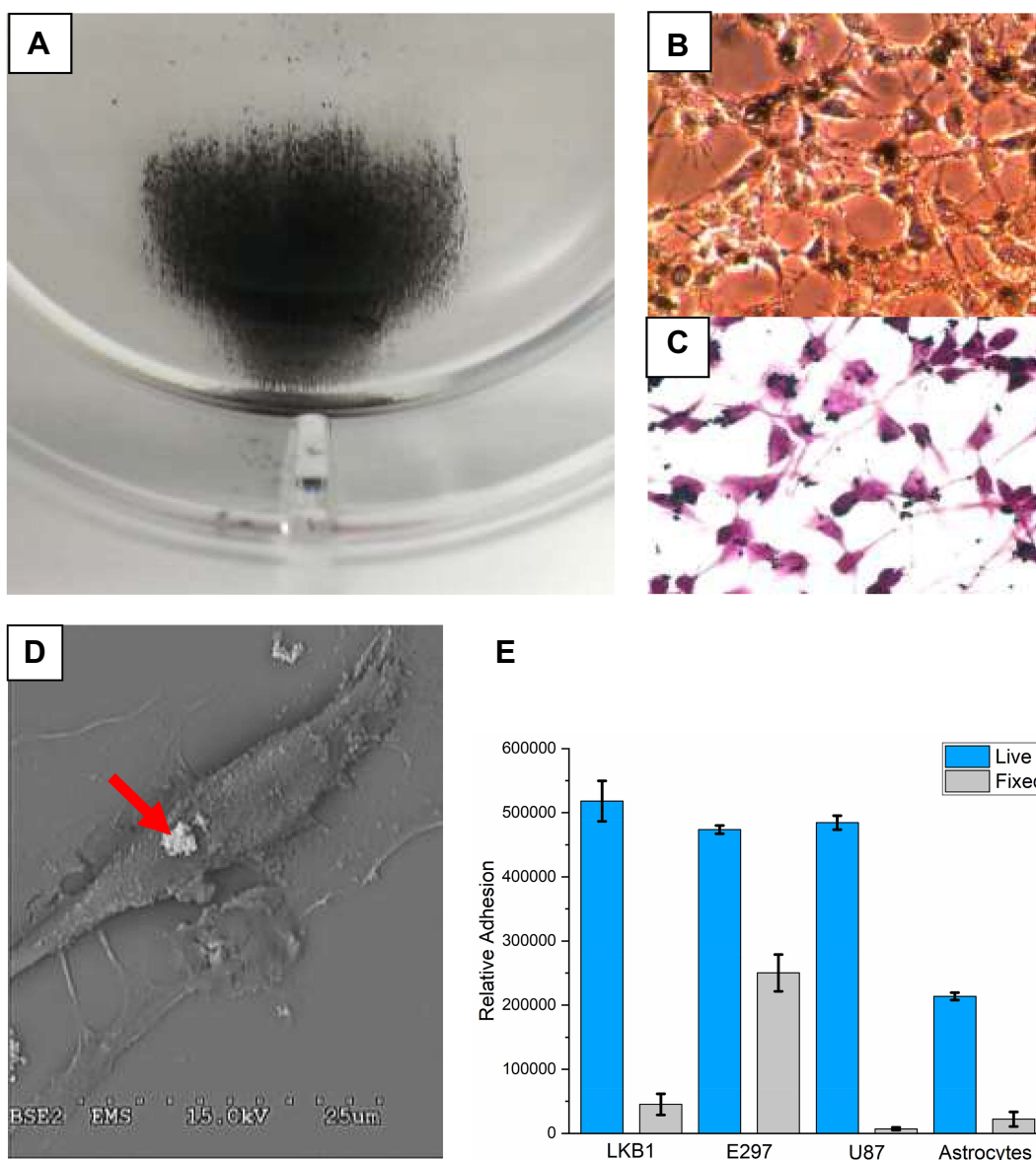


Figure 6 (A) Photograph showing the pattern of MBs as they fan out across a cellular monolayer. (B) Photomicrograph showing the adherence of MBs to live cancer cells, as seen by phase-contrast microscopy. The MB clusters are seen here as highly refractile (white) particles. (C) Photomicrograph showing the adherence of MBs to fixed cancer cells (E297, human glioblastoma), after H&E staining. (D) A scanning electron microscope (SEM) image of an MNP cluster on a glioblastoma cell (arrow). (E) Bar graph indicating the relative adherence of MBs to different types of cells, unfixed (blue) versus fixed with paraformaldehyde (gray), as quantified using ImageJ (LKB1, E297 and U87 are glioma cells; Astrocytes are not neoplastic).

methacrylate) acrylic were found to have less of a growth-inhibitory effect on U87 cells at 48 hrs, than similar pieces of VeroClear. Cells could be successfully grown in MIRT trays for up to 120 hrs, depending on the type of cell, and number of cells initially seeded.

Dynamic experiments were performed, with MBs transported down the lanes of the MIRT tray by the mini-MED, over cellular monolayers of a variety of cell types. This was to determine whether or not MB velocity would be affected differently, by different types of cells coating the lanes, and

to determine whether or not there would be particle attrition due to adhesion of particles to the walls of the lanes. A clinically relevant scenario, for instance, might be that of clusters of cancer cells seeded within the spinal subarachnoid space, which might be more adherent to drug-laden MNP clusters. Of the cell lines tested, MIRT lane velocity was the least for U138 and E297 cells, which corresponded to their high MB adhesion rates. A photomicrograph of Hoechst 33342-stained U138 cells in a lane of the MIRT tray after MBs have passed, is shown in Figure 7A. Cells are blurry at

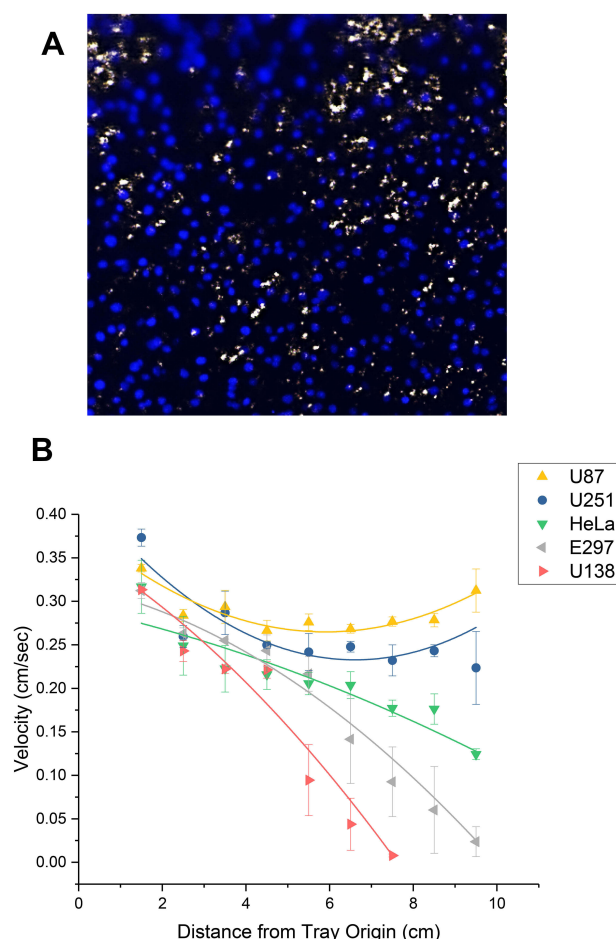


Figure 7 (A) Photomicrograph of residual (adherent) MBs in a MIRT lane containing U138 (human glioblastoma) cells. Cell nuclei were stained with Hoechst 33342. MBs clusters appear white on this image. Cells are blurry at the top of the photo, due to the curvature of the tray lane. (B) Graph showing the effect of cell type on MB velocity in the MIRT tray, in the offset above position. Different cell types were found to have different effects on the velocity and dispersion of the MB clusters.

the top of the photo, due to the curvature of the tray lane. Residual MBs can be seen adhering to the cells, as indicated in white using this technique.

The MB velocities over cellular monolayers (centimeter by centimeter) of different cell types are shown in Figure 7B. For these studies, the above offset position was used. The average velocities of MBs over HeLa, U251, U87, and E297 cells were 0.24 ± 0.02 cm/sec, 0.26 ± 0.02 cm/sec, 0.28 ± 0.01 cm/sec, and 0.18 ± 0.03 cm/sec, respectively. The attrition of MNP clusters with movement, due to MNP adhesion to the lanes, was also greater with some cells, such as U138 cells. MB movement over certain cell lines was found to be significantly slower (and with higher cluster dispersion), likely indicating their relative “stickiness”. U138 (human glioblastoma cells) for example, showed marked MNP adherence, and an 87.1% reduction in velocity (in comparison with U87 cells) at a

distance of 5.5 cm along the channel. This difference was found to be statistically significant by ANOVA, with $p < 0.05$. It would be advantageous to be able to quantify (and exploit) such adherence to cancer cells in human applications of magnetic drug targeting.

Etoposide Cytotoxicity Testing and MB Drug Transport Over Human-Sized Distances

U138 cells in wells were treated with various concentrations of the classic chemotherapeutic agent, etoposide, in order to establish parameters for assessing cytotoxic activity. Direct treatment with 100 μ M etoposide for 24 hrs (without employing the magnet) was found to decrease cellular viability to $23.0 \pm 0.4\%$, as studied by MTT assay. These results are shown in Figure 8A.

Etoposide was added to lanes at the starting points of the MIRT tray, with 60 μ L aliquots of MBs. Control lanes were also employed, which used MBs alone. MBs were remotely moved down the length of the tray (10 cm) in PBS using the mini-MED, with the tray positioned at 20 cm in the pull position. After 5 mins, MBs (with associated media) were removed from the ends of the lanes and used to treat U138 and H2122 cells for 2 hrs. Cells were analyzed for cytotoxic effect using trypan blue exclusion. Results are shown in Figure 8B and C, for U138 (human glioblastoma) and H2122 (human lung adenocarcinoma) cells, respectively. The cytotoxic effect of etoposide was retained after being delivered by MBs, and this result was found to be statistically significant ($p < 0.05$). Such an effect could not have been achieved by means of drug diffusion (with associated dilution) alone, therefore indicating the successful delivery of drug by the rotating MNP clusters.

Discussion

Data reported here show that: 1) The translational velocities of MNP clusters moving down the lanes of the MIRT tray (in response to the rotating magnet) can be roughly predicted from their clearance times in the magnetic separator; 2) Changes in the position of (or distance from) the rotating magnet predictably change the velocity of the MNPs, as does the size (i.e. mass) of the MNP aliquot; 3) Dye delivery can be used to visualize the effect of MNPs as microdevices for drug delivery; 4) MB clusters directed down MIRT tray channels lined with cells

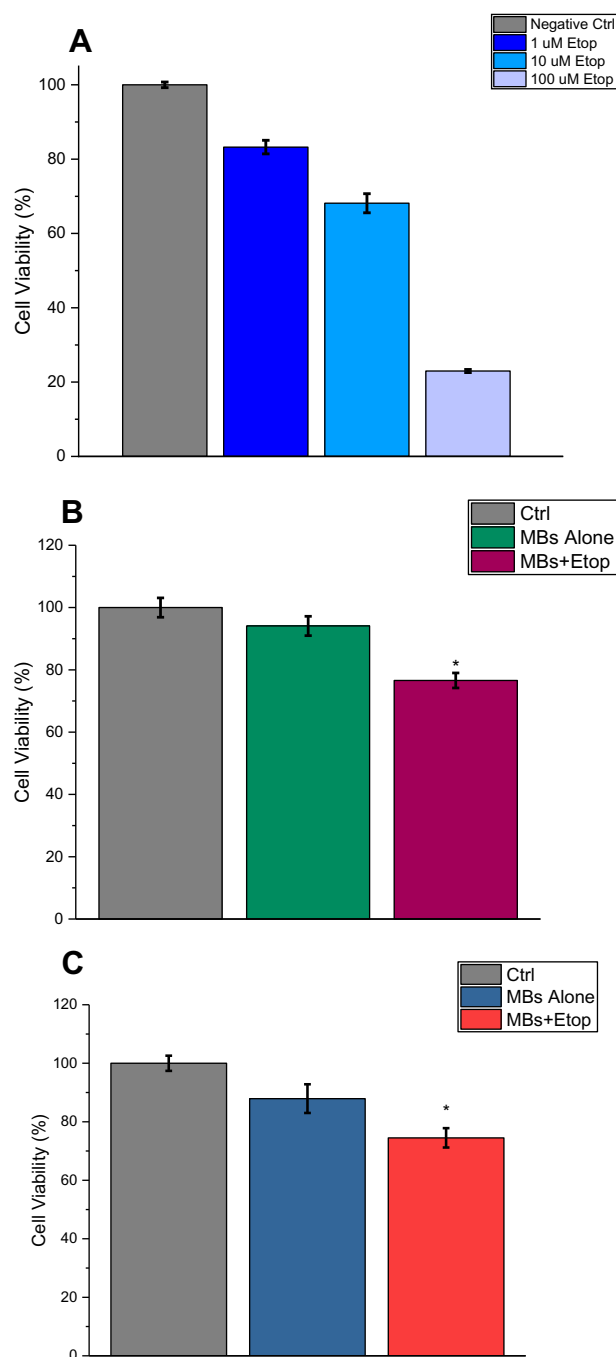


Figure 8 Etoposide cytotoxicity in static vs dynamic (MIRT tray) studies. **(A)** Viability analysis of etoposide treatment of U138 cells in a 12-well plate, as determined by MTT assay. 1 μ M, 10 μ M, and 100 μ M etoposide were used and compared to 10 μ L of DMSO (10 μ M volume equivalent) alone per well (n=3). **(B)** and **(C)** Trypan blue cell viability analyses after MBs were used to move etoposide down the lanes of the MIRT tray. **(B)** U138 (human glioblastoma) cells. **(C)** H2122 (human lung adenocarcinoma) cells. MBs successfully transported etoposide by convection/bulk flow (5 mins) to allow cancer cell killing as shown by this assay (n = 3; *p < 0.05).

exhibit varying velocities and degrees of wall adherence, depending on cell type; and 5) MB clusters can be used to enhance the delivery of the chemotherapeutic agent etoposide, across the “mesoscale” distance of 10 cm. Non-

functionalized iron oxide MNPs were studied as convective microdevices, and coating with gold and gellan gum did change the observed velocities. MBs were chosen over the other MNPs for more extensive studies, since they demonstrated the greatest velocity in response to the mini-MED. An improved velocity profile (other factors being equal) would be expected to convey an advantage in a clinical setting in which drug delivery is being augmented.

Admittedly, the in vitro model and test conditions used here are rudimentary and do poor justice to actual physiological conditions. Yet, the principles such experiments establish set the stage for achieving a more sophisticated understanding of MNP movement on a human scale, and ultimately for possible therapeutic use. Modeling of more complex conduit branching patterns in three dimensions would certainly be useful for predicting MNP movement and drug delivery within a variety of human structures and would add complexity in exponential fashion. With larger, more powerful magnets, the distance separating the magnet and MNPs could be greater, and with higher rotational speeds, the surface walking of the particles could potentially be faster. In the results reported here, MNP clusters functioned as medical devices (or “nanobots”) enhancing fluid transport for drug delivery^{11,40,41} and did not require direct drug conjugation or a mechanism for triggering drug release.

When MNPs enter an environment containing cells, they adsorb biomolecules and form a corona, assuming a biological identity which is distinct from their synthetic identity.^{42–47} The composition of the bio-corona will depend on the specific environment in which the particles are used, and can include solutes, lipids, protein, and other molecules.^{1,42,48–50} Surface charge and corona formation can be altered by nanoparticle coatings, which in turn affect nanoparticle adherence to (and uptake by) cells.^{13,51,52} Different types of cells have been studied for this effect including macrophages, fibroblasts, osteoblasts, and HeLa, neuroblastoma and ovarian cancer cells.^{44,51,53–59} Since corona formation may affect MNP targeting and drug delivery, this phenomenon provides another rationale for laboratory modeling (such as our own), prior to resource-intensive in vivo studies. The MBs studied here have been reported to rotate and display translational movement through serum and even blood,^{10,11} fluid environments shown to generate a corona. Use of the MIRT tray and mini-Med for primitive modeling of blood vessels, for analysis of tPA delivery to a blood clot, has recently been reported.¹¹

Considering MNP modeling relevant to cancer, studies have shown that a variety of chemotherapeutic drugs can be

bound to, and transported by MNPs.^{60–63} MNP-chemotherapy constructs have demonstrated growth-inhibitory effects in vitro and in animal studies for many types of cancer cells, including glioblastoma.^{2,64–66} Ingenious larger nanostructures (“micro-robots”) which can be actuated by external magnetic fields have also been described, with the goal of targeting drug delivery.^{67–70} These may or may not contain iron, or utilize a tumbling motion.^{67,71} Few reports have described the use of unbound MNP clusters (also referred to as “aggregates” or, more accurately “agglomerates”) as microdevices for delivering therapeutic agents at human-sized distances.^{11,33,72} As with solitary nanoparticle-drug conjugates, multiple strategies are envisioned that would allow MNP clusters to disperse and release drug at their target site.⁷³ Tumors demonstrate an “enhanced permeation and retention effect”, and individual tumor cells, as well, are likely to demonstrate heightened nonspecific binding and uptake of drugs and nanoparticles due to their greater metabolic needs.^{74,75} In the CNS, reports have demonstrated that magnetic particles can be moved within the CSF-containing conduit of the spinal subarachnoid space.^{76–78} These studies have employed either fixed (non-rotating) permanent magnets or static electromagnetic fields.

While the surface walking phenomenon of magnetic particles in response to a rotating or oscillating magnetic field has long been recognized, its potential clinical application for drug delivery has recently gained new appreciation.^{3,10,11,40,41} The main advantages of using a rotating permanent magnet as a magneto-motive unit (over that of a static or oscillating electromagnetic field) are that: 1) it may be able to induce MNP cluster movement at a greater distance; and 2) it can act unilaterally, i.e. it does not have to surround the target region.⁴⁰ Few animal studies have yet been reported which utilize this rotational mechanism.^{41,79} Additional data are needed regarding many important and fundamental considerations of the variables influencing rotating MNP clusters as devices for drug delivery. While the human condition entails even more complexity, a list of factors that could affect rotational magnetic drug targeting (rMDT) – just in vitro – is given in Table 2.

Clinical Applications of Rotational Magnetic Drug Targeting

MNP clusters induce drug movement in the absence of direct drug conjugation to the MNP itself. They are envisioned as acting as implantable micro-motors, which may have a capacity for being (at least partially) removed, due to their mobile,

Table 2 Variables Influencing Rotational Magnetic Drug Targeting (rMDT) in vitro (Factors May Be Redundant, Overlap, Interact)

A. MNP / Cluster	B. Tray / Lane
MNP type / size / composition / heterogeneity	Composition
MNP magnetization / zeta potential	Lane width / radius
MNP charge / coating	Smoothness / irregularity / pitting
Prior magnetic exposure	Electrostatic effects / charge
Composition of corona	Elasticity / flexibility
Particle mixture / ratios	Erosion / friability
Aggregate / cluster size	Coating
Cluster stability / disassembly	Branching / curvature
Cluster cohesion	Wall shear / margination
Torque / traction	Wall adherence
Cluster adherence / interactions	Barrier phenomena (e.g. encountering target cell cluster or clot) / reflection
Coefficients of friction: rotational	Coefficients of friction: static, dynamic
Wave phenomena / energy dissipation	
C. Media	D. Cellular lining
pH / temperature	Type / size
Viscosity / cavitation	Density / % confluence
Composition (protein, lipid, etc.)	Surface characteristics / waviness
Heterogeneity	Metabolic / endocytotic activity
Volume / depth / meniscus	Lane adherence
Cells suspended in media (e.g. RBCs, immune cells)	Cluster adherence
Bulk fluid flow / axial pulsations	Cellular mixture (e.g. endothelial plus cancer)
Webbing / matrix / scaffolds	Ciliation
E. Magnetic source	F. Drug / Miscellaneous
Distance	Drug type / size
Position / rotation (3D)	Drug charge / solubility / lipophilicity

(Continued)

Table 2 (Continued).

Speed of rotation / oscillation	Nonspecific loading / adherence to MNPs
Field strength / heterogeneity	Ratio of cluster size to lane width
Permanent vs electromagnetic	External pulsations

magnetic nature. Accordingly, the FDA approval process may be different from that of a drug–nanoparticle conjugate.^{73,75} The advantage of magnetic drug targeting (MDT) lies in its potential ability to control the concentration and distribution of drug within a desired target region. This is usually accomplished with external driving magnets, and is expected to minimize toxicity in untargeted tissue.^{29,80} Maximal pull or push forces can be used within the body to direct MNPs to precise locations, even against currents.^{38,80} To date, human trials of MDT have been restricted to a focusing depth of 5 cm.³⁸ Halbach arrays have been successfully used to optimally project magnetic forces in clinical applications.^{81,82}

While MNP clusters might not penetrate solid tissue, they may be able to directed through conduits (such as blood vessels, lymphatics, or the spinal subarachnoid space) or across surfaces (such as the uroepithelium, or peritoneal cavity).^{65,83} Potential avenues and targets for MNP delivery, including implants such as catheters, are listed in Table 3, according to organ system and medical specialty. Adhesion of particles to the wall or surface, along with margination and wall shear, are major factors in determining whether or not MNPs will be successfully directed to their targets.^{84–86} Orientation of the rotating magnet will also play a critical role, and this may need to change during targeting along a complex route. Strengths arguing for the clinical use of MNP clusters include their ability to be moved through stagnant fluid (such as to an area of obstruction), or even against flow and pulsations.^{11,17,72} Uncertainties (as with MNPs in general) include their possible long-term toxicity, and/or generation of an immune or inflammatory response.¹⁴ Within the arterial system, formation of emboli by MNP clusters could be a major concern and would have to be avoided, especially in organs such as the brain and heart, until safety was ensured. Another difficulty arises from the general incompatibility of magnets with electronic devices, especially in complex medical environments. These issues need to be further addressed experimentally.

Table 3 Applications for Remote MNP-Enhanced Drug Delivery for Representative Conduits and Surfaces in the Human Body

Specialty / System	Naturally Occurring Structure	Implanted Device	Potential Disease Application
CNS – brain	Ventricular system	VP shunt, EVD, Ommaya reservoir	Cancer, hydrocephalus, IVH
	Cerebral arterial system	Stent	Stroke
	Cerebral venous system		Venous thrombosis
	Virchow-Robin spaces		Multiple (general CNS drug delivery)
CNS – spine	Spinal subarachnoid space	Infusion pump, CSF port	Cancer, spinal cord injury, pain, etc.
GU	Bladder, kidney	Catheter	Cancer, obstruction, hemorrhage
	Ureter		Kidney stones
	Fallopian tube, seminal tubule		Conception
GI	Peritoneal cavity		Cancer, infection, endometriosis
Cardiac	Coronary arteries	Stent	MI
	Pericardium		Pericardial effusion
Vascular	Veins, arteries	Stent	Thrombosis, insufficiency
Pulmonary; thoracic	Bronchioles		Asthma
	Pleural cavity	Chest tube	Pleural effusion
Orthopedic	Joints: knee, shoulder, hip	Artificial joints	Arthritis
Ophthalmology	Retina, cornea, aqueous humor	Implants	Decreased vision, glaucoma

Abbreviations: VP, ventriculoperitoneal; EVD, external ventricular drain; IVH, intraventricular hemorrhage; MI, myocardial infarction.

MNP clusters can contain more than one type of particle. Sophisticated MNP-based drug delivery vehicles have recently been reported, which combine thermotherapy and chemotherapy with encouraging results in vitro and in lung-xenograft – bearing mice.⁸⁷ Hybrid MNPs have been developed, which allow for chemotherapy release in response to magnetically induced heating or a low-power radiofrequency field.^{88,89} Delivering such particles, or particle clusters having multiple components, via conduits by the rotational mechanism we have described, may open up new avenues for successful MDT. Magnetically enhanced delivery of chemotherapy would be expected to have greater efficacy if administered earlier in the course of cancer dissemination. Early seedings of cancer cells could possibly be treated through access afforded by the lymphatic system, genitourinary system, and peritoneal cavity, as examples. An expected early clinical application of MIRT technology in the CNS would be in the treatment of patients with leptomeningeal metastases.^{90–93} The greatest impact would be in treating (at an early stage) cancer cells disseminating via CSF from a primary brain tumor such as medulloblastoma, since systemic metastases would not have already occurred.⁹⁴

Conclusions

Rotating MNPs clusters can be used as simple microdevices for drug delivery, including chemotherapeutic agents as we demonstrate here. Precisely directing such drug carriers remains the “Holy Grail” of MDT.^{8,95} Basic factors such as magnet position and the cellular lining of the access channels must be critically analyzed by in vitro modeling in order to predict MNP behavior in vivo. Velocity and cell surface adhesion of MNP clusters can be quantified, using video photography and digital analysis. Further studies need to be performed to determine whether or not MNP clusters – or their payload – may preferentially attach to (or be taken up by) cancer cells more than non-neoplastic cells, especially in vivo. Otherwise, additional targeting and release mechanisms may be required – functions for which hybrid MNPs are well suited.⁷³ Achieving an improved understanding of the factors that influence MNP agglomeration, stability, translational movement, drug binding and release, and ultimately uptake by the target cells, will be crucial for making the jump to successful human applications of rMDT.

Acknowledgments

The authors would like to thank Hagai Ganin and Edward Jones (UIC Radiology) for their help with obtaining the CT and MRI images. We also thank Dylan Lynch (UIC

Makerspace) and Joel Rodriguez (UIC Science Instrument Shop) for assistance in milling the MIRT trays, Michelle Van Scoyk (UIC Cancer Center) for assistance with light microscopy, and Olivia Thompson (UIC Electron Microscopy) for assistance with SEM. The authors also thank Syed Hussain and Dr. Georgia Papavasiliou (Department of Bioengineering, Illinois Institute of Technology), for providing the Nanosight data. Data reported in this paper were presented at the Annual Meeting of the American Association for Cancer Research, Washington, D.C., April 2017; Frontiers in Biomagnetic Particles Conference, Asheville, North Carolina, June 2017; and the Annual Meeting of the American Association for Cancer Research, Chicago, Illinois, April 2018.

Funding

Funding for this project was through The Brain Tumor Research Fund at The University of Illinois at Chicago Cancer Center, Chicago, IL, USA.

Disclosure

Michael E Sabo was a full-time employee of Pulse Therapeutics Inc. from June 2009 to April 2019. Francis M Creighton was employed by Pulse Therapeutics Inc. Mr. Sabo and Dr. Creighton are currently employees of UNandUP, Inc., St. Louis, MO, USA. A patent “Tissue Culture Tray and System for the In Vitro Testing and Characterization of Magnetically Induced Rotation and Translational Motion of Magnetic Particles”; July 2017 US20180024109A1 was described and used in this paper. The authors report no other conflicts of interest in this work.

References

1. Laurent S, Saei AA, Behzadi S, Panahifar A, Mahmoudi M. Superparamagnetic iron oxide nanoparticles for delivery of therapeutic agents: opportunities and challenges. *Expert Opin Drug Deliv*. 2014;11(9):1449–1470. doi:10.1517/17425247.2014.924501
2. Zhu L, Zhou Z, Mao H, Yang L. Magnetic nanoparticles for precision oncology: theranostic magnetic iron oxide nanoparticles for image-guided and targeted cancer therapy. *Nanomedicine (Lond)*. 2017;12(1):73–87. doi:10.2217/nnm-2016-0316
3. Lee GP, Pernal SP, Shokuhfar T, Engelhard HH. Nanoparticles as therapeutic agents for patients with brain tumors. In: Newton H, editor. *Handbook of Brain Tumor Chemotherapy, Molecular Therapeutics and Immunotherapy*. 2nd ed. San Diego: Academic Press; 2018:229–246.
4. D'Agata F, Ruffinatti FA, Boschi S, et al. Magnetic nanoparticles in the central nervous system: targeting principles, applications and safety issues. *Molecules*. 2017;23:1. doi:10.3390/molecules23010009
5. Amreddy N, Babu A, Muralidharan R, et al. Recent advances in nanoparticle-based cancer drug and gene delivery. *Adv Cancer Res*. 2018;137:115–170. doi:10.1016/bs.acr.2017.11.003
6. Chenthamara D, Subramaniam S, Ramakrishnan SG, et al. Therapeutic efficacy of nanoparticles and routes of administration. *Biomater Res*. 2019;23:20. doi:10.1186/s40824-019-0166-x

7. Cao Q, Han X, Li L. Enhancement of the efficiency of magnetic targeting for drug delivery: development and evaluation of magnet system. *J Magn Magn Mater*. 2011;323(15):1919–1924. doi:10.1016/j.jmmm.2010.11.058
8. Shapiro B, Kulkarni S, Nacev A, Muro S, Stepanov PY, Weinberg IN. Open challenges in magnetic drug targeting. *Wiley Interdiscip Rev Nanomed Nanobiotechnol*. 2015;7(3):446–457. doi:10.1002/wnan.1311
9. Chang M, Lin Y-H, Gabayno JL, Li Q, Liu X. Thrombolysis based on magnetically-controlled surface-functionalized Fe₃O₄ nanoparticle. *Bioengineered*. 2017;8(1):29–35. doi:10.1080/21655979.2016.1227145
10. Engelhard HH, Pernal SP, Gaertner ZA, et al. A novel tissue culture tray for the study of magnetically induced rotation and translation of iron oxide nanoparticles. *IEEE Magn Lett*. 2017;8:1–5. doi:10.1109/LMAG.2017.2761818
11. Pernal S, Willis A, Sabo M, et al. An in vitro model system for evaluating remote magnetic nanoparticle movement and fibrinolysis. *Int J Nanomedicine*. 2020;15:1549–1568. doi:10.2147/IJN.S237395
12. Zhi D, Yang T, Yang J, Fu S, Zhang S. Targeting strategies for superparamagnetic iron oxide nanoparticles in cancer therapy. *Acta Biomater*. 2020;102:13–34. doi:10.1016/j.actbio.2019.11.027
13. Singh D, McMillan JM, Kabanov AV, Sokolsky-Papkov M, Gendelman HE. Bench-to-bedside translation of magnetic nanoparticles. *Nanomedicine (Lond)*. 2014;9(4):501–516. doi:10.2217/NMM.14.5
14. Bayda S, Hadla M, Palazzolo S, et al. Inorganic nanoparticles for cancer therapy: a transition from lab to clinic. *Curr Med Chem*. 2018;25(34):4269–4303. doi:10.2174/0929867325666171229141156
15. Maia FR, Reis RL, Oliveira JM. Finding the perfect match between nanoparticles and microfluidics to respond to cancer challenges. *Nanomedicine*. 2019;24:102139. doi:10.1016/j.nano.2019.102139
16. Ghosh A, Fischer P. Controlled propulsion of artificial magnetic nanostructured propellers. *Nano Lett*. 2009;9(6):2243–2245. doi:10.1021/nl900186w
17. Karle M, Wöhrle J, Miwa J, et al. Controlled counter-flow motion of magnetic bead chains rolling along microchannels. *Microfluid Nanofluidics*. 2011;10(4):935–939. doi:10.1007/s10404-010-0727-8
18. Singh H, Laibinis PE, Hatton TA. Rigid, superparamagnetic chains of permanently linked beads coated with magnetic nanoparticles: synthesis and rotational dynamics under applied magnetic fields. *Langmuir*. 2005;21(24):11500–11509. doi:10.1021/la0517843
19. Kang TG, Hulslen MA, Anderson PD, den Toonder JMJ, Meijer HEH. Chaotic mixing induced by a magnetic chain in a rotating magnetic field. *Phys Rev E*. 2007;76(6):066303. doi:10.1103/PhysRevE.76.066303
20. Petousis I, Homburg E, Derks R, Dietzel A. Transient behaviour of magnetic micro-bead chains rotating in a fluid by external fields. *Lab Chip*. 2007;7(12):1746. doi:10.1039/b713735b
21. Roy T, Sinha A, Chakraborty S, Ganguly R, Puri IK. Magnetic microsphere-based mixers for microdroplets. *Phys Fluids*. 2009;21(2):027101. doi:10.1063/1.3072602
22. Wilson RJ, Hu W, Fu CW, et al. Formation and properties of magnetic chains for 100 nm nanoparticles used in separations of molecules and cells. *J Magn Magn Mater*. 2009;321(10):1452–1458. doi:10.1016/j.jmmm.2009.02.066
23. Mørup S, Hansen MF, Frandsen C. Magnetic interactions between nanoparticles. *Beilstein J Nanotechnol*. 2010;1:182–190. doi:10.3762/bjnano.1.22
24. Ganguly R, Puri IK. Microfluidic transport in magnetic MEMS and bioMEMS. *Wiley Interdiscip Rev Nanomed Nanobiotechnol*. 2010;2(4):382–399. doi:10.1002/wnan.92
25. Etheridge ML, Hurlley KR, Zhang J, et al. Accounting for biological aggregation in heating and imaging of magnetic nanoparticles. *Technology (Singap World Sci)*. 2014;2(3):214–228. doi:10.1142/S2339547814500198
26. Wang C, Hsu CH, Li Z, et al. Effective heating of magnetic nanoparticle aggregates for in vivo nano-theranostic hyperthermia. *Int J Nanomedicine*. 2017;12:6273–6287. doi:10.2147/IJN.S141072
27. Gädke J, Thies J-W, Kleinfeldt L, et al. Selective manipulation of superparamagnetic nanoparticles for product purification and microfluidic diagnostics. *Eur J Pharm Biopharm*. 2018;126:67–74. doi:10.1016/j.ejpb.2017.09.008
28. Guibert C, Dupuis V, Peyre V, Fresnais J. Hyperthermia of magnetic nanoparticles: experimental study of the role of aggregation. *J Phys Chem C*. 2015;119(50):28148–28154. doi:10.1021/acs.jpcc.5b07796
29. Ramaswamy B, Kulkarni SD, Villar PS, et al. Movement of magnetic nanoparticles in brain tissue: mechanisms and impact on normal neuronal function. *Nanomedicine*. 2015;11(7):1821–1829. doi:10.1016/j.nano.2015.06.003
30. Mair LO, Weinberg IN, Nacev A, et al. Analysis of driven nanorod transport through a biopolymer matrix. *J Magn Magn Mater*. 2015;380:295–298. doi:10.1016/j.jmmm.2014.09.059
31. Soheilian R, Choi YS, David AE, Abdi H, Maloney CE, Erb RM. Toward accumulation of magnetic nanoparticles into tissues of small porosity. *Langmuir*. 2015;31(30):8267–8274. doi:10.1021/acs.langmuir.5b01458
32. Engelhard H, Gaertner Z, Levin A, et al. Rotating magnetic beads for enhanced drug delivery: characterization of bead velocity, imaging, and adherence to cellular monolayers, abstract 3104. *Am Assoc Cancer Res*. 2017;3104. doi:10.1158/1538-7445.AM2017-3104
33. Pouponneau P, Leroux J-C, Martel S. Magnetic nanoparticles encapsulated into biodegradable microparticles steered with an upgraded magnetic resonance imaging system for tumor chemoembolization. *Biomaterials*. 2009;30(31):6327–6332. doi:10.1016/j.biomaterials.2009.08.005
34. Pernal SP, Willis AJ, Engelhard HH. Magnetic nanoparticles (MNPs) for cancer drug delivery: the value of in vitro modeling, abstract 4661. *Am Assoc Cancer Res*. 2018;4661. doi:10.1158/1538-7445.AM2018-4661
35. Cao Q, Han X, Li L. Configurations and control of magnetic fields for manipulating magnetic particles in microfluidic applications: magnet systems and manipulation mechanisms. *Lab Chip*. 2014;14(15):2762–2777. doi:10.1039/c4lc00367e
36. Pajtler KW, Tippelt S, Siegler N, et al. Intraventricular etoposide safety and toxicity profile in children and young adults with refractory or recurrent malignant brain tumors. *J Neurooncol*. 2016;128(3):463–471. doi:10.1007/s11060-016-2133-x
37. Venugopal I, Pernal S, Duproz A, Bentley J, Engelhard H, Linninger A. Magnetic field-enhanced cellular uptake of doxorubicin loaded magnetic nanoparticles for tumor treatment. *Mater Res Express*. 2016;3(9):095010. doi:10.1088/2053-1591/3/9/095010
38. Sarwar A, Nemirovski A, Shapiro B. Optimal halbach permanent magnet designs for maximally pulling and pushing nanoparticles. *J Magn Magn Mater*. 2012;324(5):742–754. doi:10.1016/j.jmmm.2011.09.008
39. Zhu Q, Jiang L, Wang X. The expression of duffy antigen receptor for chemokines by epithelial ovarian cancer decreases growth potential. *Oncol Lett*. 2017;13(6):4302–4306. doi:10.3892/ol.2017.5954
40. Fountain TWR, Kailat PV, Abbott JJ. Wireless control of magnetic helical microrobots using a rotating-permanent-magnet manipulator. In: 2010 IEEE International Conference on Robotics and Automation; 2010; Anchorage, AK: IEEE: 576–581. doi:10.1109/ROBOT.2010.5509245
41. Cheng R, Huang W, Huang L, et al. Acceleration of tissue plasminogen activator-mediated thrombolysis by magnetically powered nanomotors. *ACS Nano*. 2014;8(8):7746–7754. doi:10.1021/nn5029955
42. Lundqvist M, Stigler J, Elia G, Lynch I, Cedervall T, Dawson KA. Nanoparticle size and surface properties determine the protein corona with possible implications for biological impacts. *Proc Natl Acad Sci USA*. 2008;105(38):14265–14270. doi:10.1073/pnas.0805135105
43. Walczyk D, Bombelli FB, Monopoli MP, Lynch I, Dawson KA. What the cell “sees” in bionanoscience. *J Am Chem Soc*. 2010;132(16):5761–5768. doi:10.1021/ja910675v
44. Walkey CD, Chan WCW. Understanding and controlling the interaction of nanomaterials with proteins in a physiological environment. *Chem Soc Rev*. 2012;41(7):2780–2799. doi:10.1039/c1cs15233e

45. Lesniak A, Salvati A, Santos-Martinez MJ, Radomski MW, Dawson KA, Åberg C. Nanoparticle adhesion to the cell membrane and its effect on nanoparticle uptake efficiency. *J Am Chem Soc.* **2013**;135(4):1438–1444. doi:10.1021/ja309812z
46. Calatayud MP, Sanz B, Raffa V, Riggio C, Ibarra MR, Goya GF. The effect of surface charge of functionalized Fe₃O₄ nanoparticles on protein adsorption and cell uptake. *Biomaterials.* **2014**;35(24):6389–6399. doi:10.1016/j.biomaterials.2014.04.009
47. Docter D, Strieth S, Westmeier D, et al. No king without a crown—impact of the nanomaterial-protein corona on nanobiomedicine. *Nanomedicine (Lond).* **2015**;10(3):503–519. doi:10.2217/nnm.14.184
48. Raesch SS, Tenzer S, Störck W, et al. Proteomic and lipidomic analysis of nanoparticle corona upon contact with lung surfactant reveals differences in protein, but not lipid composition. *ACS Nano.* **2015**;9(12):11872–11885. doi:10.1021/acsnano.5b04215
49. Yang H, Wang M, Zhang Y, et al. Detailed insight into the formation of protein corona: conformational change, stability and aggregation. *Int J Biol Macromol.* **2019**;135:1114–1122. doi:10.1016/j.ijbiomac.2019.06.014
50. Gräfe C, von der Lühse M, Weidner A, et al. Protein corona formation and its constitutional changes on magnetic nanoparticles in serum featuring a polydehydroalanine coating: effects of charge and incubation conditions. *Nanotechnology.* **2019**;30(26):265707. doi:10.1088/1361-6528/ab0ed0
51. Hanot CC, Choi YS, Anani TB, Soundararajan D, David AE. Effects of iron-oxide nanoparticle surface chemistry on uptake kinetics and cytotoxicity in CHO-K1 cells. *Int J Mol Sci.* **2015**;17:1. doi:10.3390/ijms17010054
52. Sobczynski DJ, Charoenphol P, Heslinga MJ, et al. Plasma protein corona modulates the vascular wall interaction of drug carriers in a material and donor specific manner. *PLoS One.* **2014**;9(9):e107408. doi:10.1371/journal.pone.0107408
53. Villanueva A, Cañete M, Roca AG, et al. The influence of surface functionalization on the enhanced internalization of magnetic nanoparticles in cancer cells. *Nanotechnology.* **2009**;20(11):115103. doi:10.1088/0957-4484/20/11/115103
54. Tsai ZT, Tsai FY, Yang WC, et al. Preparation and characterization of ferrofluid stabilized with biocompatible chitosan and dextran sulfate hybrid biopolymer as a potential magnetic resonance imaging (MRI) T2 contrast agent. *Mar Drugs.* **2012**;10(11):2403–2414. doi:10.3390/md10112403
55. Luengo Y, Nardecchia S, Morales MP, Serrano MC. Different cell responses induced by exposure to maghemite nanoparticles. *Nanoscale.* **2013**;5(23):11428–11437. doi:10.1039/c3nr02148c
56. Arcella A, Palchetti S, Digiacoio L, et al. Brain targeting by liposome-biomolecular corona boosts anticancer efficacy of temozolomide in glioblastoma cells. *ACS Chem Neurosci.* **2018**;9(12):3166–3174. doi:10.1021/acscchemneuro.8b00339
57. Vogt C, Pernemalm M, Kohonen P, et al. Proteomics analysis reveals distinct corona composition on magnetic nanoparticles with different surface coatings: implications for interactions with primary human macrophages. *PLoS One.* **2015**;10(10):e0129008. doi:10.1371/journal.pone.0129008
58. Gräfe C, Weidner A, Lühse MV, et al. Intentional formation of a protein corona on nanoparticles: serum concentration affects protein corona mass, surface charge, and nanoparticle-cell interaction. *Int J Biochem Cell Biol.* **2016**;75:196–202. doi:10.1016/j.biocel.2015.11.005
59. Grumezescu V, Gherasim O, Negut I, et al. Nanomagnetite-embedded PLGA spheres for multipurpose medical applications. *Materials (Basel).* **2019**;12(16). doi:10.3390/ma12162521
60. Xing R, Wang X, Zhang C, et al. Superparamagnetic magnetite nanocrystal clusters as potential magnetic carriers for the delivery of platinum anticancer drugs. *J Mater Chem.* **2011**;21(30):11142. doi:10.1039/c1jm11369k
61. Sundaresan V, Menon JU, Rahimi M, Nguyen KT, Wadajkar AS. Dual-responsive polymer-coated iron oxide nanoparticles for drug delivery and imaging applications. *Int J Pharm.* **2014**;466(1–2):1–7. doi:10.1016/j.ijpharm.2014.03.016
62. Cicha I, Scheffler L, Ebenau A, Lyer S, Alexiou C, Goppelt-Strube M. Mitoxantrone-loaded superparamagnetic iron oxide nanoparticles as drug carriers for cancer therapy: uptake and toxicity in primary human tubular epithelial cells. *Nanotoxicology.* **2016**;10(5):557–566. doi:10.3109/17435390.2015.1095364
63. Liu M-C, Jin S-F, Zheng M, et al. Daunomycin-loaded superparamagnetic iron oxide nanoparticles: preparation, magnetic targeting, cell cytotoxicity, and protein delivery research. *J Biomater Appl.* **2016**;31(2):261–272. doi:10.1177/0885328216654425
64. Alexiou C, Jurgons R, Schmid RJ, et al. Magnetic drug targeting—biodistribution of the magnetic carrier and the chemotherapeutic agent mitoxantrone after locoregional cancer treatment. *J Drug Target.* **2003**;11(3):139–149. doi:10.1080/1061186031000150791
65. Pouponneau P, Soulez G, Beaudoin G, Leroux J-C, Martel S. MR imaging of therapeutic magnetic microcarriers guided by magnetic resonance navigation for targeted liver chemoembolization. *Cardiovasc Intervent Radiol.* **2014**;37(3):784–790. doi:10.1007/s00270-013-0770-4
66. Zhang H, Liu XL, Zhang YF, et al. Magnetic nanoparticles based cancer therapy: current status and applications. *Sci China Life Sci.* **2018**;61(4):400–414. doi:10.1007/s11427-017-9271-1
67. Kim S, Qiu F, Kim S, et al. Fabrication and characterization of magnetic microrobots for three-dimensional cell culture and targeted transportation. *Adv Mater Weinheim.* **2013**;25(41):5863–5868. doi:10.1002/adma.201301484
68. Sun M, Fan X, Meng X, et al. Magnetic biohybrid micromotors with high maneuverability for efficient drug loading and targeted drug delivery. *Nanoscale.* **2019**;11(39):18382–18392. doi:10.1039/c9nr06221a
69. Mair LO, Evans BA, Nacev A, et al. Magnetic microkayaks: propulsion of microrods precessing near a surface by kilohertz frequency, rotating magnetic fields. *Nanoscale.* **2017**;9(10):3375–3381. doi:10.1039/c6nr09459g
70. Mair LO, Chowdhury S, Paredes-Juarez GA, et al. Magnetically aligned nanorods in alginate capsules (maniacs): soft matter tumbling robots for manipulation and drug delivery. *Micromachines.* **2019**;10(4). doi:10.3390/mi10040230
71. Lee S, Kim S, Nelson B, Choi H. Fabrication and targeted particle delivery using microrobots. 12th International Conference on Ubiquitous Robots and Ambient Intelligence. Gyeongju City, Korea, October **2015**.
72. Bonnacaze R, Clements M. Multi-scale model of magnetically-driven flows in dead-end channels. XXIV ICTAM; August; **2016**; Montreal, Canada.
73. Tietze R, Zaloga J, Unterwiesing H, et al. Magnetic nanoparticle-based drug delivery for cancer therapy. *Biochem Biophys Res Commun.* **2015**;468(3):463–470. doi:10.1016/j.bbrc.2015.08.022
74. Pillai G, Ceballos-Coronel ML. Science and technology of the emerging nanomedicines in cancer therapy: a primer for physicians and pharmacists. *SAGE Open Med.* **2013**;1:2050312113513759. doi:10.1177/2050312113513759
75. Pillai G. Nanomedicines for cancer therapy: an update of FDA approved and those under various stages of development. *SOJPPS.* **2014**. doi:10.15226/2374-6866/1/2/00109
76. Engelhard HH, Petruska DA. Imaging and movement of iron-oxide-bound antibody microparticles in brain and cerebrospinal fluid. *Cancer Biochem Biophys.* **1992**;13(1):1–12.
77. Venugopal I, Habib N, Linninger A. Intrathecal magnetic drug targeting for localized delivery of therapeutics in the CNS. *Nanomedicine (Lond).* **2017**;12(8):865–877. doi:10.2217/nmm-2016-0418
78. Husain SF, Lam RWM, Hu T, et al. Locating the site of neuropathic pain in vivo using MMP-12-targeted magnetic nanoparticles. *Pain Res Manag.* **2019**;2019:9394715. doi:10.1155/2019/9394715
79. Huang L, Wang J, Huang S, Siaw-Debrah F, Nyanzu M, Zhuge Q. Polyacrylic acid-coated nanoparticles loaded with recombinant tissue plasminogen activator for the treatment of mice with ischemic stroke. *Biochem Biophys Res Commun.* **2019**;516(2):565–570. doi:10.1016/j.bbrc.2019.06.079

80. Nacev A, Komae A, Sarwar A, et al. Towards control of magnetic fluids in patients: directing therapeutic nanoparticles to disease locations. *IEEE Control Syst.* **2012**;32(3):32–74. doi:10.1109/MCS.2012.2189052
81. Creighton FM, Ritter RC, Werp P. Focused magnetic navigation using optimized magnets for medical therapies. Magnetics Conference, 2005. INTERMAG Asia 2005. Digests of the IEEE International; **2005**. pp. 1253–1254.
82. Creighton FM Optimal distribution of magnetic material for catheter and guidewire cardiology therapies. Magnetics Conference, 2006. INTERMAG 2006. IEEE International; **2006**. pp. 111.
83. Shamsi M, Sedaghatkish A, Dejam M, Saghaian M, Mohammadi M, Sanati-Nezhad A. Magnetically assisted intraperitoneal drug delivery for cancer chemotherapy. *Drug Deliv.* **2018**;25(1):846–861. doi:10.1080/10717544.2018.1455764
84. Haun JB, Hammer DA. Quantifying nanoparticle adhesion mediated by specific molecular interactions. *Langmuir.* **2008**;24(16):8821–8832. doi:10.1021/la8005844
85. Kim MJ, Rhee K. Computational analysis of nanoparticle adhesion to endothelium: effects of kinetic rate constants and wall shear rates. *Med Biol Eng Comput.* **2011**;49(7):733–741. doi:10.1007/s11517-011-0735-1
86. Carboni E, Tschudi K, Nam J, Lu X, Ma AWK. Particle margination and its implications on intravenous anticancer drug delivery. *AAPS PharmSciTech.* **2014**;15(3):762–771. doi:10.1208/s12249-014-0099-6
87. Liu D, Hong Y, Li Y, et al. Targeted destruction of cancer stem cells using multifunctional magnetic nanoparticles that enable combined hyperthermia and chemotherapy. *Theranostics.* **2020**;10(3):1181–1196. doi:10.7150/thno.38989
88. Louguet S, Rousseau B, Epherre R, et al. Thermoresponsive polymer brush-functionalized magnetic manganite nanoparticles for remotely triggered drug release. *Polym Chem.* **2012**;3(6):1408. doi:10.1039/c2py20089a
89. Peiris PM, Abramowski A, McGinnity J, et al. Treatment of invasive brain tumors using a chain-like nanoparticle. *Cancer Res.* **2015**;75(7):1356–1365. doi:10.1158/0008-5472.CAN-14-1540
90. Barshes N, Demopoulos A, Engelhard HH. Anatomy and physiology of the leptomeninges and CSF space. *Cancer Treat Res.* **2005**;125:1–16. doi:10.1007/0-387-24199-x_1
91. Raja A, Engelhard HH. Animal models of leptomeningeal cancer. *Cancer Treat Res.* **2005**;125:159–179. doi:10.1007/0-387-24199-x_10
92. Willis A, Karumudi B, Liu B, et al. A novel etoposide-bound magnetic nanoparticle for remote targeting of cancer cells. *Cancer Res.* **2019**;79(Suppl 13):2166. doi:10.1158/1538-7445.AM2019-2166
93. Le Rhun E, Preusser M, van den Bent M, Andratschke N, Weller M. How we treat patients with leptomeningeal metastases. *ESMO Open.* **2019**;4(Suppl 2):e000507. doi:10.1136/esmoopen-2019-000507
94. Kwasnicki A, Lakka S, Willis A, et al. Development of a new etoposide-bound magnetic nanoparticle designed to treat medulloblastoma cells disseminated within cerebrospinal fluid pathways. *Neuro Oncol.* **2019**;21(Suppl 2):ii113. doi:10.1093/neuonc/noz036.203
95. Nacev A, Weinberg IN, Stepanov PY, et al. Dynamic inversion enables external magnets to concentrate ferromagnetic rods to a central target. *Nano Lett.* **2015**;15(1):359–364. doi:10.1021/nl503654t

International Journal of Nanomedicine

Publish your work in this journal

The International Journal of Nanomedicine is an international, peer-reviewed journal focusing on the application of nanotechnology in diagnostics, therapeutics, and drug delivery systems throughout the biomedical field. This journal is indexed on PubMed Central, MedLine, CAS, SciSearch®, Current Contents®/Clinical Medicine,

Submit your manuscript here: <https://www.dovepress.com/international-journal-of-nanomedicine-journal>

Journal Citation Reports/Science Edition, EMBase, Scopus and the Elsevier Bibliographic databases. The manuscript management system is completely online and includes a very quick and fair peer-review system, which is all easy to use. Visit <http://www.dovepress.com/testimonials.php> to read real quotes from published authors.